Antibacterial Activity and CO_2 Capture by Cerium-Copper Mixed Oxides Prepared Using a Co-precipitation Method

Sirilak Kamonwannasit[1], Cybelle Morales Futalan[2], Pongtanawat Khemthong[3], Saran Youngjan[3], and Piaw Phatai[4*]

[1]*Department of Agro-Industrial Product Development, Faculty of Agricultural Technology, Burapha University, Sakaeo 27160, Thailand*

[2]*Institute of Civil Engineering, University of the Philippines, Diliman Quezon City 1101, Philippines*

[3]*National Nanotechnology Center (NANOTEC), National Science and Technology Development Agency (NSTDA), Pathum Thani 12120, Thailand*

[4]*Department of Chemistry, Faculty of Science, Udon Thani Rajabhat University, Udon Thani 41000, Thailand*

* ***Corresponding author:***

email: piaw.ph@udru.ac.th

Received: September 10, 2023
Accepted: March 31, 2024

DOI: 10.22146/ijc.88872

Abstract: *Indoor air pollution is comprised of fine particles, bacteria, fungi, and hydrocarbons. Acceptable indoor air quality is maintained using several layers of air filters. Alternative materials with the capacity to remove CO_2 from indoor air with antibacterial efficacy need to be further investigated. Mixed oxides of $Ce_{1.0-x}Cu_xO$ (x = 0.0, 0.1, 0.5, 0.9, 1.0) were synthesized using a co-precipitation method. Characterization studies revealed that single oxides of $Ce_{1.0}O$ and $Cu_{1.0}O$ were of cubic fluorite and monoclinic crystal structures, respectively. Results also show that $Ce_{0.1}Cu_{0.9}O$ and $Ce_{0.5}Cu_{0.5}O$ were composites. All samples were classified as mesoporous materials with a type IV isotherm, and the main functional group was identified as Ce–O–Cu. The surface area of $Ce_{0.5}Cu_{0.5}O$ was 17.63 m^2/g. The highest CO_2 adsorption capacity was 5.72 cm^3/g for $Ce_{0.5}Cu_{0.5}O$. Moreover, the greatest antibacterial activity against* B. subtilis *(12.22 mm inhibition zone) and* P. aeruginosa *(7.34 mm inhibition zone) was observed for $Ce_{0.5}Cu_{0.5}O$ at a 30 mg/L concentration. The synthesis of mixed $Ce_{1.0-x}Cu_xO$ oxides along with their satisfactory antibacterial performance and CO_2 adsorption capacity, indicate its potential use as an alternative material for inclusion in indoor air filters.*

Keywords: *mixed oxide; cerium; copper; co-precipitation; CO_2 capture*

■ INTRODUCTION

Indoor air quality and its effects on human health have always been a concern since people spend about 87% of their time inside their homes and workplaces [1]. Indoor air quality has been determined to contain higher concentration of air pollutants when compared to outdoor air quality due to confined spaces and limited ventilation [2]. Indoor air pollution is a heterogeneous mixture of many substances including bacteria, particulate matter, carbon dioxide (CO_2), ozone, and volatile organic compounds. Particulate matter is typically comprised of sulfates, nitrates, organic carbon, metal ions, and microbial particles [3]. Enclosed spaces with poor ventilation and the presence of bacteria in indoor air give rise to respiratory diseases in humans [4]. Additionally, air filters that entrap bacteria can also serve as its culture site. Greenhouse gasses such as CO_2 have detrimental effects on human health such as decreased cognitive level, asphyxia, sore eyes, high blood pressure, and chest pain when present in indoor air in elevated concentrations [5]. High CO_2 concentrations are found in indoor environments ranging from 1000 to 3000 ppm compared to outdoor CO_2 with an average concentration of 415 ppm [6]. The maximum allowable concentration of CO_2 is 600 ppm in the United States for indoor air, while a maximum concentration of

1000 ppm is acceptable in Singapore, Korea, Japan, and China [7]. Hence, air treatment is needed to remove microbes and chemical pollutants and maintain indoor air quality.

There are several types of air filters that can remove a variety of air pollutants including microbes, chemical contaminants, and particulate matters [8]. Air filters can be modified in several ways, including surface chemical modification, UV treatment, ion method, and integration with nanoparticles [9-10]. The study of Krishnamurthy et al. [11] synthesized tetraethylenepentamine-based latex paint with a CO_2 adsorptive capacity of 48.4 mg/g. In the work of Wicaksono et al., molecular sieve 13X zeolite particles with a diameter size of 1 nm were integrated into air filters and provided 316 mg/L reduction in indoor CO_2 using 140 g of zeolite [12]. Several types of conventional filters can attain high removal efficiency for pathogens and other air pollutants, which makes air purifier systems expensive and bulky. Therefore, researchers have focused on the development of multifunctional air filters with high antibacterial activity and the capacity to remove chemical contaminants.

Metal oxide nanoparticles (NPs) with antibacterial properties that can also remove other air contaminants can be incorporated into air filters. Recently, NPs have gained attention due to their extensive potential applications in nanodevices, nanosensors, nanoelectronics, and heat transfer fluids. Cerium oxide (CeO_2) nanoparticles have been utilized in various applications, including biomedicine [13-14], catalysis [15-16], environmental applications [17], and fuel cells [18]. The acid-base property of CeO_2, with its highly reactive surface, makes it an excellent material for removing CO_2 from the air. The study of Slostowski et al. [17] developed CeO_2 particles using supercritical alcohols as surface modifiers for CO_2 capture. Li et al. [19] utilized a surfactant-template method to synthesize CeO_2 NPs with a CO_2 capture capacity of 30 mg/g. Metal oxides such as ZrO_2, Al_2O_3, SiO_2, and CeO_2 were investigated by Yoshikawa et al. [20], and their corresponding adsorption capacities for CO_2 were determined. Another characteristic of CeO_2 is its catalytic activity, which is also related to the reversible reaction between redox pairs of Ce^{3+} and Ce^{4+}. More oxygen vacancies are present if there is excess Ce^{3+} in CeO_2, which favors a quick oxygen exchange process. A higher fraction of Ce^{3+} is generally observed with smaller CeO_2 particle sizes. The unique redox properties of CeO_2 have been utilized to protect normal human cells. Additionally, CeO_2 has cytotoxic effects on bacteria due to its oxidation-reduction potential, which inhibits ATP activity, affecting the transport of nutrients and causing oxidative stress [21].

To improve the antibacterial properties of CeO_2, a second metal oxide can be introduced into the nanoparticle structure. Copper oxide (CuO) is characterized by its useful physical properties, such as photocatalytic characteristics, thermal stability, electron correlation effects, spin dynamics, superconductivity at high temperatures, and anti-microbial and anti-fungal properties [22]. There are numerous applications of CuO NPs in batteries, gas sensors, catalysis, adsorbents, antibacterial agents and fuel cells. The photocatalytic properties of CuO are attributed to its crystal structure and narrow bandgap energy. Copper-doped CeO_2 has been utilized in several studies as a catalyst for the oxidation of CO [23-25] and ethene [26], as well as a humidity sensor [27]. The incorporation of cerium (Ce^{3+}–Ce^{4+}) oxide into copper (Cu^{+}–Cu^{2+}) oxide creates a synergistic effect during oxidation reactions. CuO and CeO_2 can be simultaneously reduced and oxidized where the presence of CuO increases the redox mechanism at the catalyst surface. The study of Dosa et al. [23] shows an improved oxidation performance for ethylene and CO using cerium-CuO.

Several methods of the synthesis of CuO and CeO_2 were evaluated including impregnation method [28], emulsion polymerization method [29], surfactant template method [30], and hydrothermal method [31]. However, several drawbacks include complex set-up, utilization of organic solvents that are deleterious in nature and requirement of high temperature [32]. Meanwhile, co-precipitation is a single-step process that operates at low temperature and utilizes green reagents. So far, there are no reports on mixed oxides of Ce and Cu as possible materials in air filters that take advantage of their antibacterial properties and CO_2 capture capacity.

In this work, cerium-copper mixed oxides $Ce_{1.0-x}Cu_xO$ (x = 0.0, 0.1, 0.5, 0.9, and 1.0) were developed by a simple co-precipitation method, which is controllable and facile. The physicochemical properties of the mixed oxides, such as their crystal phase structure and surface morphology, were determined using various techniques including XRD, FTIR, SEM-EDX, and N_2 adsorption/desorption isotherms. An agar well diffusion technique was used to study the antibacterial activity of cerium-copper mixed oxides. Additionally, the CO_2 capture capacity of CeCuO was evaluated using Autosorb for micropore analysis.

■ EXPERIMENTAL SECTION

Materials

Raw materials for CeCuO synthesis including cerium nitrate hexahydrate ($Ce(NO_3)_3{\cdot}6H_2O$, 99.5 wt.%, Acros), copper nitrate ($Cu(NO_3)_2$, 98.0 wt.%, Ajax Finechem), polyethylene glycol 4000 (PEG 4000, Merck), sodium hydroxide (NaOH, 99.0 wt.%, QReC), and an ammonia solution (NH_3, 30 wt.%, Carlo Erba) were used in this experiment. The Gram-positive bacteria, *S. aureus* (TISTR 1466) and *B. subtilis* (TISTR 008) and the Gram-negative bacterium, *P. aeruginosa* (TISTR 781), were obtained from the Thailand Institute of Scientific and Technological Research. Nutrient agar slants were used for microbe cultivation.

Instrumentation

A BELSORP-Mini X was utilized to analyze the N_2 adsorption-desorption isotherms of CeCuO at a liquid nitrogen temperature of –196 °C. Before analysis, samples were dried at 110 °C overnight and degassed at 120 °C under vacuum for 3 h. The specific surface area of CeCuO was measured within the range of a 0–1 relative pressure (P/P_0) using a Brunauer–Emmett–Teller (BET) method, while the pore size distribution through the cylindrical pore model was determined *via* the Barrett–Joyner–Halenda (BJH) desorption method. The functional groups in CeCuO were determined using FTIR spectroscopy (Spectrum Two, Perkin Elmer, USA) combined with an ATR method in the scan range of 4000–500 cm^{-1} with a resolution of 4 cm^{-1}. The crystal phases of the CeCuO were evaluated via XRD (D8 Advance Series 2, Bruker, Germany) operated at an emission current of 35 mA, an accelerating voltage of 40 kV, 2θ range from 20 to 80°, and with Cu Kα radiation (λ = 1.54184 Å).

Procedure

Synthesis of CeCuO mixed oxides

Co-precipitation method was utilized to synthesize mixed oxide particles of $Ce_{1.0-x}Cu_xO$ (x = 0.0, 0.1, 0.5, 0.9, and 1.0), referred to as CeCuO. Table 1 shows the precursors used in this synthesis. First, $Ce(NO_3)_3{\cdot}6H_2O$, $Cu(NO_3)_2$, and PEG 4000 were dissolved separately in DI water. Then, $Cu(NO_3)_2$ solution was added dropwise into the $Ce(NO_3)_3{\cdot}6H_2O$ solution. After that, PEG 4000 solution was added to the mixture and the resulting blue solution was stirred continuously for 15 min. Next, the adjustment of solution pH to 8.0 ± 0.2 was done using an NH_3 solution. This was followed by adding 1.5 M NaOH in a dropwise manner to the mixture until a pH of 12.0 ± 0.2 was achieved. Then, the mixture was stirred continuously for 30 min until precipitates were formed. The precipitates were filtered through Whatman No. 93 filter paper. Any unreacted species were removed by washing repeatedly with *n*-butyl alcohol. Then, the filtered powders were dried in an oven at 110 °C for 5 h and finally calcined at 600 °C for 4 h. $Ce_{1.0-x}Cu_xO$ (x = 0.0, 0.1, 0.5, 0.9, and 1.0) are referred to as $Ce_{1.0}O$, $Ce_{0.9}Cu_{0.1}O$, $Ce_{0.5}Cu_{0.5}O$, $Ce_{0.1}Cu_{0.9}O$ and $Cu_{1.0}O$, respectively.

Antibacterial activity

An agar well diffusion method was used to determine the antibacterial activity of the CeCuO. The bacterial strains, *P. aeruginosa*, *S. aureus* and *B. subtilis*, were grown in a Mueller-Hinton broth (MHB) for 18 h under a 0.5 turbidity (McFarland standard) at 37 °C.

Table 1. Mass of precursors for the CeCuO synthesis

Sample	Mass (g)		
	$Ce(NO_3)_3{\cdot}6H_2O$	$Cu(NO_3)_2$	PEG-4000
$Cu_{1.0}O$	-	9.3782	1.0
$Ce_{0.1}Cu_{0.9}O$	2.1711	8.4402	1.0
$Ce_{0.5}Cu_{0.5}O$	10.8555	4.6890	1.0
$Ce_{0.9}Cu_{0.1}O$	19.5399	0.9378	1.0
$Ce_{1.0}O$	21.7110	-	1.0

Each 100 µL bacterial suspension, with a cell count of 1×10^8 CFU/mL, was uniformly spread on individual MHB agar plates. Wells with diameters of 5 mm were cut using a sterile cork borer. Next, CeCuO aliquots (50 µL) were dropped in each well. Finally, the inoculated plates were incubated for 24 h at 37 °C. Tetracycline (30 µg) and dimethyl sulfoxide (DMSO) were used as positive and negative controls, respectively. Last, the widths of bacterial inhibition zones were measured. Triplicate runs of all experiments were performed.

CO_2 adsorption experiment

The adsorption experiments of CO_2 were performed using an Autosorb for micropore analysis (Autosorb IQ3). Prior to each adsorption experiment, CeCuO samples were degassed at 200 °C for 5 h under helium gas to remove impurities and then cooled to the required temperature of 30 °C. Finally, ultrahigh purity CO_2 (99.999%) was introduced into the system at 30 °C with pressures of 0–1 bar.

■ RESULTS AND DISCUSSION

Material Characterization

Fig. 1(a) shows the lattice parameters and crystal phases of CeO_2 and CuO in CeCuO calcined at 600 °C for 4 h. The presence of 2θ peaks in $Cu_{1.0}O$ was observed at 2θ = 35.74°, 38.95°, 49.21°, 61.79°, 66.22°, 68.42°, and 75.37° that correspond to the (-111), (111), (-202), (-113), (022), (220), and (004) planes, respectively (JCPDS No. 01-1117). This result indicates a typical CuO monoclinic structure within the *C2/c* space group. Several 2θ peaks were observed in the XRD pattern of $Ce_{1.0}O$ at 28.68°, 33.28°, 47.83°, 56.78°, 76.34°, and 79.03°, which correspond to the (111), (200), (220), (311), (331) and (420) planes, respectively (JCPDS No. 01-0800). This result represents a typical CeO_2 cubic fluorite structure within the *Fm-3m* space group. The XRD patterns of $Ce_{0.1}Cu_{0.9}O$ and $Ce_{0.5}Cu_{0.5}O$ exhibited mixed phases of CeO_2 and CuO. However, the XRD pattern of $Ce_{0.9}Cu_{0.1}O$ displayed only the CeO_2 phase, indicating that CeO_2 and CuO are not present in simple composite forms of the individual Ce and Cu oxides. Instead, they are found in the form of a solid solution with metal ions inserted within the CeO_2 crystal structure. This is due to differences in the ionic radii of Ce^{3+}, Ce^{4+}, and Cu^{2+}, which are 0.114, 0.097, and 0.073 nm, respectively. The smaller ionic radius of Cu^{2+} ions may cause the substitution of Cu^{2+} for Ce^{4+} within the crystal lattice of CeO_2 [33-34]. Moreover, the very low quantity of copper in $Ce_{0.9}Cu_{0.1}O$ makes the detection of a CuO peak impossible.

The average crystallite sizes (D) of CeO_2 and CuO in CeCuO were calculated using the Debye Scherrer as shown in Eq. (1);

$$D = \frac{k\lambda}{\beta \cos\theta} \quad (1)$$

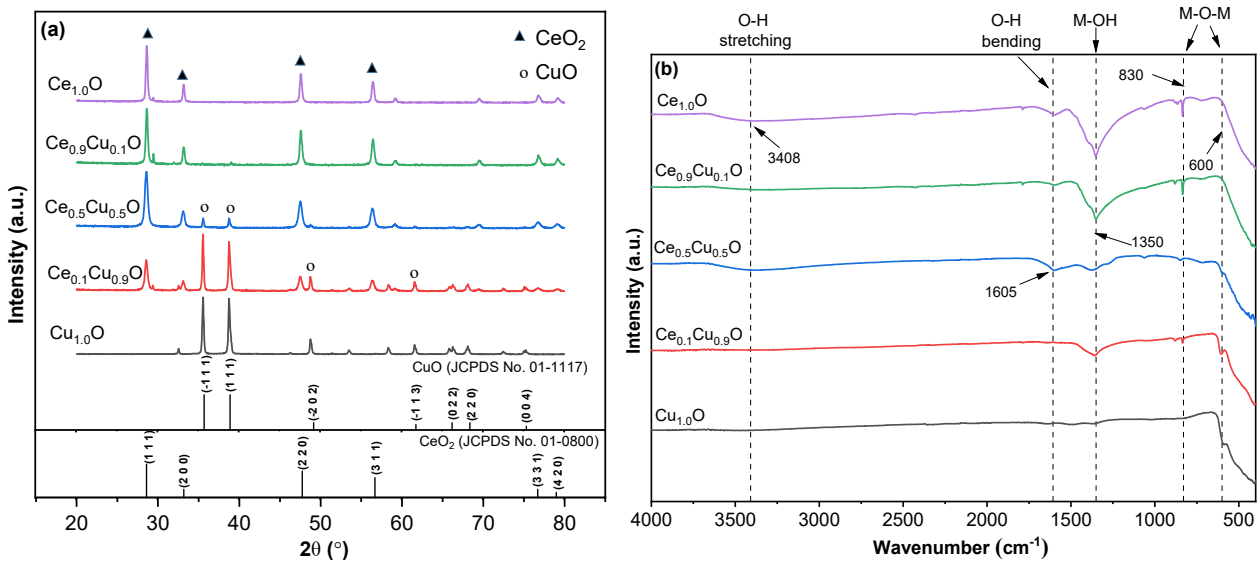

Fig 1. (a) XRD pattern and (b) FTIR spectra of CeCuO samples calcined at 600 °C for 4 h

where k refers to the broadening constant that changes with crystal type, θ (°) refers to the Bragg diffraction angle, β (radians) is the full width at half maximum (FWHM) of a given reflection, and λ is the wavelength of Cu Kα radiation (λ = 0.15418 nm).

The peaks at (111), (200), (220), (311), and (420) reflections, which show no interference, were used to calculate the crystallite size of CeO_2 in CeCuO. Table 2 shows that the crystallite size of CeO_2 in all samples (except for $Cu_{1.0}O$) gradually increases with the Ce content. The crystallite size increased from 33 nm ($Ce_{0.1}Cu_{0.9}O$) to 68 nm ($Ce_{1.0}O$). The peaks at (-111), (111), (-202), and (-113) were used to compute the crystallite size of CuO. These results showed that the CuO sizes were in the range of 45–77 nm. However, the size of CuO in $Ce_{0.9}Cu_{0.1}O$ could not be determined because of the very low amount of copper.

The lattice parameter (a) and unit cell volume (V_{cell}) of CeO_2 in CeCuO are calculated using Eq. (2) and (3), respectively [35];

$$\frac{1}{d_{hkl}^2} = \left(\frac{h^2 + k^2 + l^2}{a^2}\right) \quad (2)$$

$$V_{cell} = a^3 \quad (3)$$

where d_{hkl} represents the lattice distance between (hkl) planes in a cubic crystal; h, k and l refer to the crystallographic indices, and a refers to the crystallographic lattice parameters. The main peaks at (111), (200), (220), and (311) were used to compute the a value of CeO_2 in CeCuO. Table 2 reveals that a and V_{cell} values of CeO_2 in $Ce_{1.0}O$ were 0.54 nm and 0.158 nm^3, respectively. The values of the lattice parameters obtained were similar to that in previous literature [35]. Moreover, the a and V_{cell} values of CeO_2 in CeCuO were identical to those of $Ce_{1.0}O$. This result suggests that the introduction of copper ions into CeO_2 lattice does not induce substantial structural modifications at the atomic level.

Fig. 1(b) shows the FTIR spectra of CeCuO samples. The broad peak at 3408 cm^{-1} corresponds to stretching vibrations, and the weak absorption band at 1623 cm^{-1} is attributed to the bending vibrations of absorbed molecular water on the specimen surfaces [36]. The strong band at 1350 cm^{-1} can possibly be ascribed to M–OH (M = Ce, Cu) vibrations [37]. The 830 and 600 cm^{-1} peaks correspond to the symmetric deformation vibrations of metal-oxygen and metal-oxygen-metal networks (M–O–M; M = Ce, Cu) [38]. This suggests that atomic connectivity was present in CeCuO. Additionally, the 600 cm^{-1} peak is attributed to the CuO band [39].

Fig. 2 demonstrates the N_2 adsorption-desorption isotherms and pore size distributions of CeCuO. All isotherms were classified as type IV that indicates a H_3-type hysteresis loops. As shown in Table 2, the S_{BET} of $Ce_{1.0}O$ and $Cu_{1.0}O$ are 10.28 and 3.38 m^2/g, respectively. The total pore volume and pore diameters of the samples were in the range of 0.020–0.200 cm^3/g and 20–45 nm, respectively. This implies that the synthesized CeCuO is a mesoporous material. $Ce_{0.5}Cu_{0.5}O$ presented the highest surface area and pore volume with values of 17.63 m^2/g and 0.1736 cm^3/g, respectively. This could affect the different samples' antibacterial activity and CO_2

Table 2. Structural properties of the CeCuO samples obtained from XRD analysis and N_2 adsorption-desorption isotherms

Sample	D[a] (nm)		S[b]BET	D_{AV}	V[c]	a	V_{cell}
	CeO_2	CuO	(m^2/g)	(nm)	(cm^3/g)	(nm)	(nm^3)
$Cu_{1.0}O$	-	45.50	3.38	24.67	0.0209	-	-
$Ce_{0.1}Cu_{0.9}O$	33.45	76.85	6.32	29.60	0.0468	0.5406	0.158
$Ce_{0.5}Cu_{0.5}O$	45.55	59.95	17.63	39.38	0.1736	0.5406	0.158
$Ce_{0.9}Cu_{0.1}O$	58.55	-	3.36	43.24	0.0362	0.5400	0.157
$Ce_{1.0}O$	68.10	-	10.28	34.16	0.0878	0.5406	0.158

[a]Scherrer's equation to estimate the crystallite size
[b]Bruneuer-Emmett-Teller (BET) method used to determine specific surface area
[c]Barrett-Joyner-Halenda (BJH) method used to determine the total pore volume
D_{AV} is the average pore diameter (BJH adsorption)

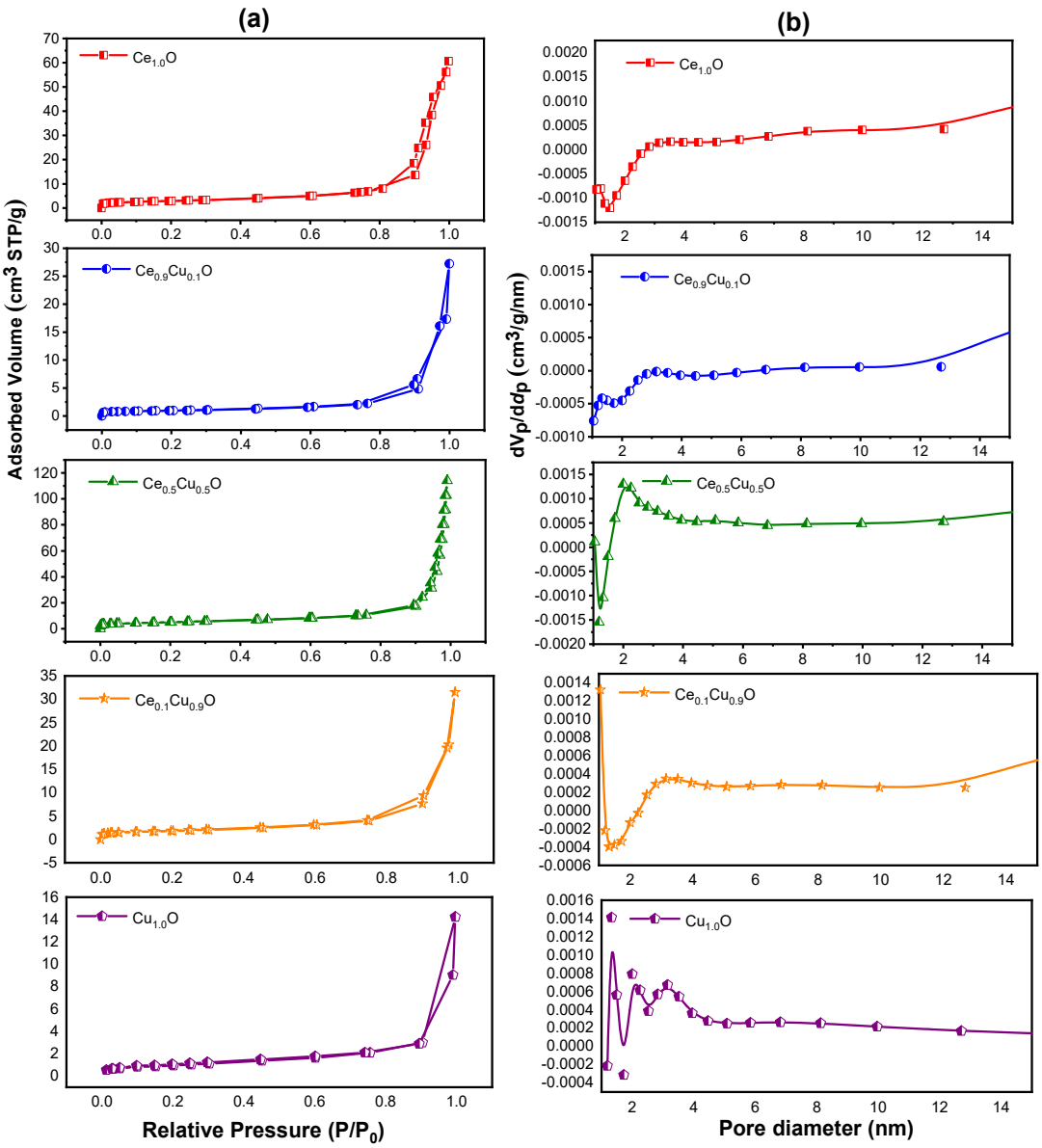

Fig 2. (a) N_2 adsorption-desorption isotherms and (b) pore size distribution of CeCuO samples calcined at 600 °C for 4 h

adsorption, which will be further discussed in subsequent sections.

Antibacterial Activity

The antibacterial activity of CeCuO at 10 and 30 mg/mL concentrations was studied against three strains of bacteria using an agar well diffusion method. Widths of inhibition zones were measured to evaluate antibacterial performance. A larger zone of inhibition indicates higher susceptibility to an antibacterial agent. Table 3 and Fig. 3 show the width of inhibition zones around wells with CeCuO particles against three bacterial strains after incubation for 24 h. Results show that tetracycline was effective against all strains of bacteria, with inhibition zones ranging from 16–24 mm. However, no inhibition zones were observed for DMSO. The appearance of bacterial growth for all samples at 10 mg/mL indicates that there is no antibacterial activity against any of the strains at this concentration. Based on previous studies, CeO_2 NPs do not have significant antibacterial activity. The study of Syed Khadar et al. [40] showed that CeO_2 and cobalt-doped CeO_2 NPs synthesized *via* hydrothermal technique did not have any

Table 3. Width of inhibition zones of the synthesized CeCuO samples against three bacterial strains

Type of bacteria	Inhibition diameter (mm) (10 mg/mL)	Inhibition diameter (mm) (30 mg/mL)	Inhibition diameter (mm) for tetracycline (30 μg)
$Cu_{1.0}O$			
S. aureus	ND	ND	–
B. subtilis	ND	11.04±0.23	–
P. aeruginosa	ND	ND	–
$Ce_{0.1}Cu_{0.9}O$			
S. aureus	ND	ND	–
B. subtilis	ND	11.13±0.79	–
P. aeruginosa	ND	ND	–
$Ce_{0.5}Cu_{0.5}O$			
S. aureus	ND	ND	–
B. subtilis	ND	12.22±0.17	–
P. aeruginosa	ND	7.34±0.05	–
$Ce_{0.9}Cu_{0.1}O$			
S. aureus	ND	ND	–
B. subtilis	ND	ND	–
P. aeruginosa	ND	ND	–
$Ce_{1.0}O$			
S. aureus	ND	ND	–
B. subtilis	ND	ND	–
P. aeruginosa	ND	ND	–
Tetracycline			
S. aureus	–	–	23.66 ± 0.50
B. subtilis	–	–	16.71 ± 2.23
P. aeruginosa	–	–	19.15 ± 0.47

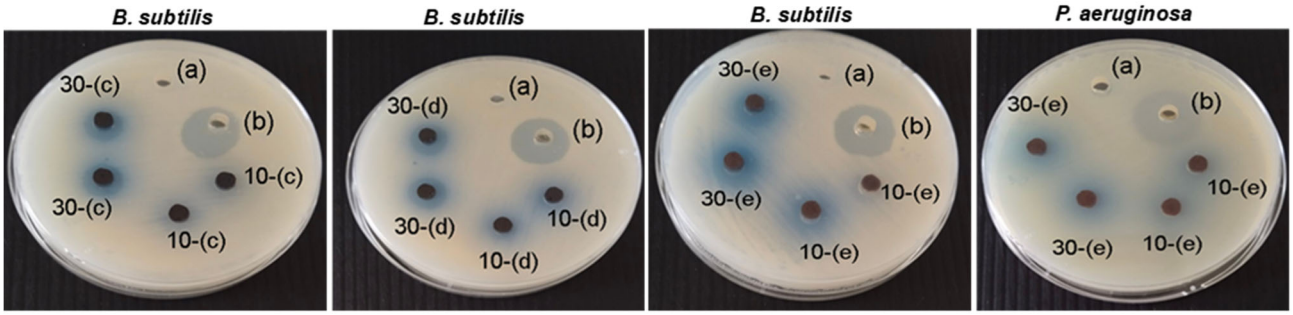

Fig 3. Photographs of the antibacterial activity of calcined samples against gram-negative bacteria *P. aeruginosa* and gram-positive bacteria *B. subtilis* at a dose of 10 and 30 mg/mL: (a) negative control, (b) positive control, (c) $Cu_{1.0}O$, (d) $Ce_{0.1}Cu_{0.9}O$ and (e) $Ce_{0.5}Cu_{0.5}O$

activity against bacteria [40]. CeO_2 nanoparticles synthesized using laser ablation in liquid showed no growth inhibition for bacteria even at 700 μg/mL [41].

In the present study, inhibition zones were formed at concentration of 30 mg/mL of $Cu_{1.0}O$ and $Ce_{0.1}Cu_{0.9}O$ with widths ranging from 11–12 mm for only *B. subtilis*. For $Ce_{0.5}Cu_{0.5}O$ at a dose of 30 mg/L, all strains except *S. aureus* formed zones of inhibition that were between 7–12 mm in width. Moreover, the strain of the Gram-negative bacterium, *P. aeruginosa*, was inhibited only

using $Ce_{0.5}Cu_{0.5}O$ at 30 mg/L. The antimicrobial activity of CeCuO NPs is attributed to the release Cu and Ce ions, which could generate reactive oxygen species that would break cell membranes and cell walls and react with protein and DNA [42]. Results showed that a Gram-positive bacterium (*B. subtilis*) was more susceptible than Gram-negative bacteria. This likely occurred since the cell walls of Gram-positive bacteria are comprised of lipoteichoic acids and one layer of peptidoglycan [43-44]. However, Gram-negative bacteria have multi-layered cell walls characterized by low permeability [45], which makes these strains more difficult to treat with antibiotics. Additionally, Gram-negative bacteria possess numerous efflux pumps that prevent the accumulation of antimicrobial substances in cell membranes [45].

Studies on CO_2 Uptake

Adsorption of CO_2 onto CeCuO was studied. Fig. 4(a) shows the adsorption capacity for CO_2 by CeCuO. The greatest CO_2 adsorption was observed for $Ce_{0.5}Cu_{0.5}O$ at 5.72 cm^3/g followed by $Ce_{1.0}O$ (4.57 cm^3/g), $Ce_{0.1}Cu_{0.9}O$ (4.09 cm^3/g) and $Cu_{1.0}O$ (2.65 cm^3/g). $Ce_{0.9}Cu_{0.1}O$ (2.56 cm^3/g) displayed the lowest adsorption, half that of $Ce_{0.5}Cu_{0.5}O$. These results can be correlated with the BET surface area of CeCuO materials, as shown in Fig. 4(b). $Ce_{0.5}Cu_{0.5}O$ presented the largest surface area and pore volume, which implies there is a larger surface and volume for the adsorption of CO_2. This led to high interaction between CO_2 molecules and the adsorbent surface.

In this study, the maximum adsorption capacity of CO_2 on $Ce_{0.5}Cu_{0.5}O$ was 5.72 cm^3/g at 30 °C. This value is comparable to those of CuO (9.0 cm^3/g) and Cu_2O (2.1 cm^3/g) [46]. This may have occurred due to a low affinity to CO_2 to interact with the surface of Ce–O–Cu. In general, many factors including temperature, pressure and the purity of the feed gas as well as the nature of the adsorbent (surface area, pore volume, pore size, adsorbent forms and chemistry of adsorbent) impact CO_2 adsorption [47]. Greater surface area, pore size, and volume result in higher adsorption capacity. The surface area and pore diameter of $Ce_{0.5}Cu_{0.5}O$ (17.63 m^2/g and 39.38 nm) synthesized in our work were higher than those of CuO (4.21 m^2/g and 35.2 nm) and Cu_2O (1.36 m^2/g and 9.89 nm) [46]. However, $Ce_{0.5}Cu_{0.5}O$ presented a higher CO_2 capture capacity than Cu_2O but a lower capacity than CuO. Moreover, Zeng et al. [47] reported that the dispersion of cerium oxygen species affected CO_2 adsorption. CeO_{x-5}/bio-C, having a surface area of 16.7 m^2/g, has the greatest CO_2 adsorption capacity (122.88 μmol/g or 2.50 cm^3/g), which is lower than $Ce_{0.5}Cu_{0.5}O$. These could be due to different experimental conditions involving the gas flow rate, degassing temperature, and degassing duration.

Based on literature reviews [48-49], the possible adsorption mechanism of CO_2 onto the CeCuO composite

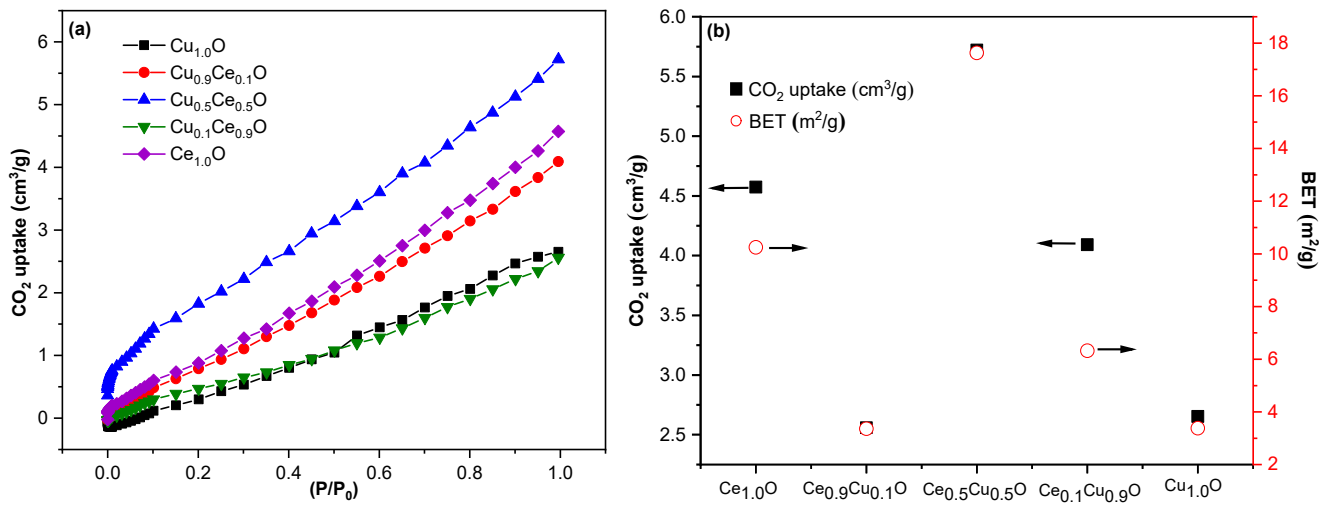

Fig 4. (a) Equilibrium adsorption capacity of CO_2 at 30 °C by CeCuO samples calcined at 600 °C for 4 h and (b) comparison between CO_2 uptake capacity and surface area CeCuO samples

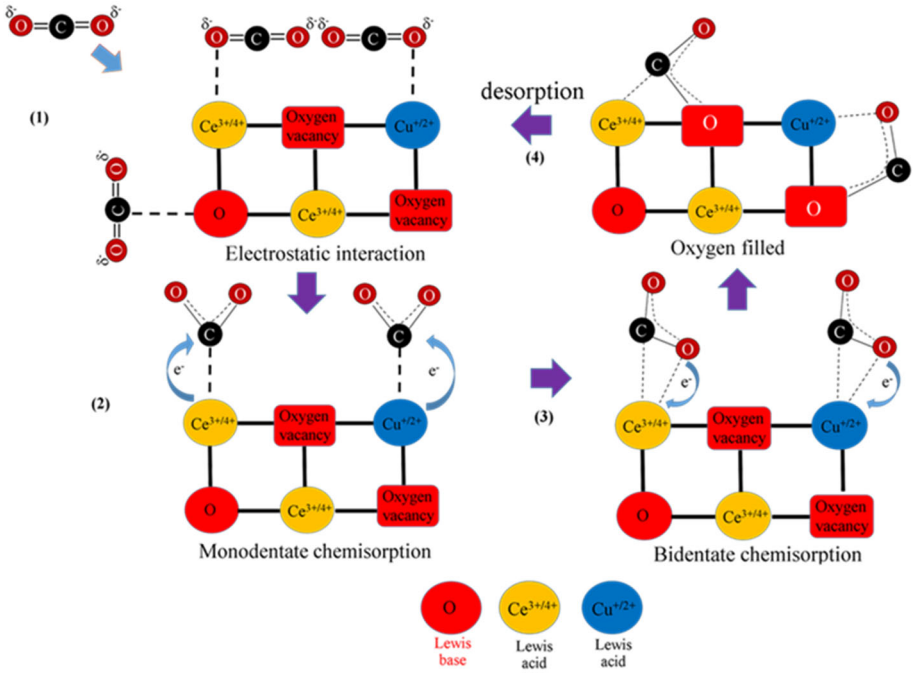

Fig 5. Possible adsorption mechanism of CO_2 on CeCuO

is depicted in Fig. 5. Adsorption begins with electrostatic interaction between CO_2 and the Ce–Cu–O network (Fig. 5(1)), where $Ce^{3+/4+}$ and $Cu^{+/2+}$ ions are acidic sites, while O^{2-} ions are basic sites. CO_2 molecules are adsorbed onto Ce and Cu through monodentate chemisorption, and then electrons from Ce and Cu are transferred to C atoms (Fig. 5(2)). After that, bidentate chemisorption takes place through the interactions of OC–O···$Ce^{3+/4+}$, O_2C···$Ce^{3+/4+}$, and O–C–O···$Cu^{+/2+}$, O_2C···$Cu^{+/2+}$ and electrons from O^{2-} delocalized to Ce and Cu (Fig. 5(3)). Finally, adsorbed oxygen atoms simply filled the oxygen vacancies (Fig. 5(4)).

■ CONCLUSION

Mixed oxide $Ce_{1.0-x}Cu_xO$ (x = 0.0, 0.1, 0.5, 0.9 and 1.0) composites were synthesized using a co-precipitation method and characterized using XRD, FTIR, and N_2-adsorption/desorption isotherms. $Ce_{0.1}Cu_{0.9}O$ and $Ce_{0.5}Cu_{0.5}O$ clearly showed mixed phases of CuO and CeO_2, indicating their composite form. The main functional group of the composites was Ce–O–Cu. All CeCuO samples are classified as mesoporous materials with the type IV isotherm. $Ce_{0.5}Cu_{0.5}O$ composite showed the highest antibacterial activity against *B. subtilis* and *P. aeruginosa*. Moreover, the highest adsorption capacity for CO_2 was attained using the $Ce_{0.5}Cu_{0.5}O$ composite. The excellent antibacterial performance and adsorption capacity of $Ce_{0.5}Cu_{0.5}O$ can be attributed to its large surface area (17.63 m^2/g) and pore diameter (39.38 nm). In general, results show the possibility of the application of $Ce_{0.5}Cu_{0.5}O$ as a potential material in air filters for indoor spaces.

■ ACKNOWLEDGMENTS

The authors would like to thank the Department of Chemistry, Faculty of Science, Udon Thani Rajabhat University for providing the spectroscopy analysis. We also thank Professor Dr. Jeffrey C. Nash from the Office of Graduate Studies of the Udon Thani Rajabhat University for his support in proofreading this manuscript.

■ AUTHOR CONTRIBUTIONS

Sirilak Kamonwannasit: Data curation, formal analysis, writing-reviewing, and editing. Cybelle Morales Futalan, Pongtanawat Khemthong, and Saran Youngjan: Methodology, Supervision, Funding acquisition. Piaw Phatai: Conceptualization, supervision, funding acquisition, writing, reviewing and editing, and project administration. All authors have read and agreed to the published version of the manuscript.

REFERENCES

[1] Salim, S.Y., Kaplan, G.G., and Madsen, K.L., 2014, Air pollution effects on the gut microbiota, *Gut Microbes*, 5 (2), 215–219.

[2] López, L.R., Dessì, P., Cabrera-Codony, A., Rocha-Melogno, L., Kraakman, N.J.R., Balaguer, M.D., and Puig, S., 2024, Indoor CO_2 direct air capture and utilization: Key strategies towards carbon neutrality, *Cleaner Eng. Technol.*, 20, 100746.

[3] Klepeis, N.E., Nelson, W.C., Ott, W.R., Robinson, J.P., Tsang, A.M., Switzer, P., Behar, J.V., Hern, S.C., and Engelmann, W.H., 2001, The National Human Activity Pattern Survey (NHAPS): A resource for assessing exposure to environmental pollutants, *J. Exposure Sci. Environ. Epidemiol.*, 11 (3), 231–252.

[4] Jankowska, E., Reponen, T., Willeke, K., Grinshpun, S.A., and Choi, K.J., 2000, Collection of fungal spores on air filters and spore reentrainment from filters into air, *J. Aerosol Sci.*, 31 (8), 969–978.

[5] Halpern, P., Raskin, Y., Sorkine, P., and Oganezov, A., 2004, Exposure to extremely high concentrations of carbon dioxide: A clinical description of a mass casualty incident, *Ann. Emerg. Med.*, 43 (2), 196–199.

[6] López, L.R., Dessì, P., Cabrera-Codony, A., Rocha-Melogno, L., Kraakman, B., Naddeo, V., Balaguer, M.D., and Puig, S., 2022, CO_2 in indoor environments: From environmental and health risk to potential renewable carbon source, *Sci. Total Environ.*, 856, 159088.

[7] Abdul-Wahab, S.A., Chin Fah En, S., Elkamel, A., Ahmadi, L., and Yetilmezsoy, K., 2015, A review of standards and guidelines set by international bodies for the parameters of indoor air quality, *Atmos. Pollut. Res.*, 6 (5), 751–767.

[8] Souzandeh, H., Wang, Y., Netravali, A.N., and Zhong, W.H., 2019, Towards sustainable and multifunctional air-filters: A review on biopolymer-based filtration materials, *Polym. Rev.*, 59 (4), 651–686.

[9] Feng, S., Li, D., Low, Z., Liu, Z., Zhong, Z., Hu, Y., Wang, Y., and Xing, W., 2017, ALD-seeded hydrothermally-grown Ag/ZnO nanorod PTFE membrane as efficient indoor air filter, *J. Membr. Sci.*, 531, 86–93.

[10] Vaterrodt, A., Thallinger, B., Daumann, K., Koch, D., Guebitz, G.M., and Ulbricht, M., 2016, Antifouling and antibacterial multifunctional polyzwitterion/enzyme coating on silicone catheter material prepared by electrostatic layer-by-layer assembly, *Langmuir.*, 32 (5), 1347–1359.

[11] Krishnamurthy, A., Salunkhe, B., Zore, A., Rownaghi, A., Schuman, T., and Rezaei, F., 2019, Amine-based latex coatings for indoor air CO_2 control in commercial buildings, *ACS Appl. Mater. Interfaces*, 11 (18), 16594–16604.

[12] Wicaksono, M.R., Handayani, I.P., Andiani, L., Chandra, I., Muminati, S.A., Kusuma Wardhani, N.P.E., and Verasta, T., 2024, Molecular sieve 13X activated zeolite for CO_2 filter in air purifier, *Mater. Today: Proc.*, In Press, Corrected Proof.

[13] Maleki, P., Nemati, F., Gholoobi, A., Hashemzadeh, A., Sabouri, Z., and Darroudi, M., 2021, Green facile synthesis of silver-doped cerium oxide nanoparticles and investigation of their cytotoxicity and antibacterial activity, *Inorg. Chem. Commun.*, 131, 108762.

[14] Zhang, H., Qiu, J., Yan, B., Liu, L., Chen, D., and Liu, X., 2021, Regulation of Ce(III)/Ce(IV) ratio of cerium oxide for antibacterial application, *iScience*, 24 (3), 102226.

[15] Cui, Z., Zhang, L., Xue, Y., Feng, Y., Wang, M., Chen, J., Ji, B., Wang, C., and Xue, Y., 2022, Effects of shape and particle size on the photocatalytic kinetics and mechanism of nano-CeO_2, *Int. J. Miner., Metall. Mater.*, 29 (12), 2221–2231.

[16] Li, G., Wen, P., Gao, C., Zhang, T., Hu, J., Zhang, Y., Guan, S., Li, Q., and Li, B., 2021, Effects of CeO_2 pre-calcined at different temperatures on the performance of Pt/CeO_2–C electrocatalyst for methanol oxidation reaction, *Int. J. Miner., Metall. Mater.*, 28 (7), 1224–1232.

[17] Slostowski, C., Marre, S., Dagault, P., Babot, O., Toupance, T., and Aymonier, C., 2017, CeO_2 nanopowders as solid sorbents for efficient CO_2 capture/release processes, *J. CO_2 Util.*, 20, 52–58.

[18] Tinh, V.D.C., Thuc, V.D., and Kim, D., 2021, Chemically sustainable fuel cells via layer-by-layer

fabrication of sulfonated poly(arylene ether sulfone) membranes containing cerium oxide nanoparticles, *J. Membr. Sci.*, 634, 119430.

[19] Li, M., Tumuluri, U., Wu, Z., and Dai, S., 2015, Effect of dopants on the adsorption of carbon dioxide on ceria surfaces, *ChemSusChem*, 8 (21), 3651–3660.

[20] Yoshikawa, K., Sato, H., Kaneeda, M., and Kondo, J.N., 2014, Synthesis and analysis of CO_2 adsorbents based on cerium oxide, *J. CO_2 Util.*, 8, 34–38.

[21] Cao, F., Zhang, Y., Sun, Y., Wang, Z., Zhang, L., Huang, Y., Liu, C., Liu, Z., Ren, J., and Qu, X., 2018, Ultrasmall nanozymes isolated within porous carbonaceous frameworks for synergistic cancer therapy: Enhanced oxidative damage and reduced energy supply, *Chem. Mater.*, 30 (21), 7831–7839.

[22] El-Trass, A., ElShamy, H., El-Mehasseb, I., and El-Kemary, M., 2012, CuO nanoparticles: Synthesis, characterization, optical properties and interaction with amino acids, *Appl. Surf. Sci.*, 258 (7), 2997–3001.

[23] Dosa, M., Marin-Figueredo, M.J., Sartoretti, E., Novara, C., Giorgis, F., Bensaid, S., Fino, D., Russo, N., and Piumetti, M., 2022, Cerium-copper oxides synthesized in a multi-inlet vortex reactor as effective nanocatalysts for CO and ethene oxidation reactions, *Catalysts*, 12 (4), 364.

[24] Pakharukova, V.P., Moroz, E.M., Kriventsov, V.V., Zyuzin, D.A., Kosmambetova, G.R., and Strizhak, P.E., 2009, Copper–cerium oxide catalysts supported on monoclinic zirconia: Structural features and catalytic behavior in preferential oxidation of carbon monoxide in hydrogen excess, *Appl. Catal., A*, 365 (2), 159–164.

[25] Papavasiliou, J., 2019, Interaction of atomically dispersed gold with hydrothermally prepared copper-cerium oxide for preferential CO oxidation reaction, *Catal. Today*, 357, 684–693.

[26] Vigneselvan, S., Manikandan, V., Petrila, I., Vanitha, A., and Chandrasekaran, J., 2020, Effect of copper substitution on structural, optical and humidity-sensing characteristics of cerium oxide nanoparticles, *J. Phys. Chem. Solids,* 136, 109173.

[27] Phatai, P., Futalan, C.M., Utara, S., Khemthong, P., and Kamonwannasit, S., 2018, Structural characterization of cerium-doped hydroxyapatite nanoparticles synthesized by an ultrasonic-assisted sol-gel technique, *Results Phys.*, 10, 956–963.

[28] Zeng, S., Zhang, L., Jiang, N., Gao, M., Zhao, X., Yin, Y., and Su, H., 2015. Multi-wall carbon nanotubes as support of copper-cerium composite for preferentially oxidation of carbon monoxide, *J. Power Sources*, 293, 1016–1023.

[29] Arango-Díaz, A., Cecilia, J.A., dos Santos-Gómez, L., Marrero-López, D., Losilla, E.R., Jiménez-Jiménez, J, and Rodríguez-Castellón, E., 2015. Characterization and performance in preferential oxidation of CO of CuO-CeO_2 catalysts synthesized using polymethyl metacrylate (PMMA) as template, *Int. J. Hydrogen Energy*, 40 (34), 11254–11260.

[30] Zeng, S., Wang, Y., Ding, S., Sattler, J.J.H.B., Borodina, E., Zhang, L., Weckhuysen, B.M., and Su, H., 2014, Active sites over CuO/CeO_2 catalysts for preferential CO oxidation, *J. Power Sources*, 256, 301–311.

[31] Gu, D., Jia, C.J., Bongard, H., Spliethoff, B., Weidenthaler, C., Schmidt, W., and Schüth, F., 2014, Ordered mesoporous Cu-Ce-O catalysts for preferential CO oxidation in H_2-rich gases: Influence of copper content and pretreatment conditions, *Appl. Catal., B*, 152-153, 11–18.

[32] Aseena, S., Abraham, N., and Suresh Babu, V., 2023, Morphological and optical studies of zinc doped cerium oxide nanoparticles prepared by single step co-precipitation method, *Mater. Today: Proc.*, 80, 1901–1905.

[33] Yudharma, G., Kurniawan, B., Rahman, I.K., and Razaq, D.S., 2019, Effect of copper substitution on the structural, morphology, and magnetic properties of $La_{0.7}Ba_{0.1}Sr_{0.2}Mn_{1-x}Cu_xO_3$ (x = 0, 0.10) manganite, *AIP Conf. Proc.*, 2168, 020011.

[34] Shabanian, M., Hajibeygi, M., and Raeisi, A., 2020, "2 - FTIR characterization of layered double hydroxides and modified layered double hydroxides" in *Layered Double Hydroxide Polymer Nanocomposites,* Eds. Thomas, S., and Daniel, S., Woodhead Publishing, Cambridge, MA, US, 77–101.

[35] Norbert, A., Alappatt, S.M., John, S.S., Shaji, S., Remillard, S.K., Deshpande, U.P., and Reena Philip, R., 2023, Phytosynthesized Cu-doped cerium oxide nanoparticles for antibacterial application, *Phys. Status Solidi A*, 220 (6), 2200731.

[36] Hospodarova, V., Singovszka, E., and Stevulova, N., 2018, Characterization of cellulosic fibers by FTIR spectroscopy for their further implementation to building materials, *Am. J. Anal. Chem.*, 9 (6), 303–310.

[37] Jayaramudu, T., Varaprasad, K., Pyarasani, R.D., Reddy, K.K., Kumar, K.D., Akbari-Fakhrabadi, A., Mangalaraja, R.V., and Amalraj, J., 2019, Chitosan capped copper oxide/copper nanoparticles encapsulated microbial resistant nanocomposite films, *Int. J. Biol. Macromol.*, 128, 499–508.

[38] Silhavy, T.J., Kahne, D., and Walker, S., 2010, The bacterial cell envelope, *Cold Spring Harbor Perspect. Biol.*, 2 (5), a000414.

[39] Szentirmai, É., Massie, A.R., and Kapás, L., 2021, Lipoteichoic acid, a cell wall component of Gram-positive bacteria, induces sleep and fever and suppresses feeding, *Brain, Behav., Immun.*, 92, 184–192.

[40] Syed Khadar, Y.A., Balamurugan, A., Devarajan, V.P., Subramanian, R., and Dinesh Kumar, S., 2019, Synthesis, characterization and antibacterial activity of cobalt doped cerium oxide (CeO_2:Co) nanoparticles by using hydrothermal method, *J. Mater. Res. Technol.*, 8 (1), 267–274.

[41] Abid, S.A., Taha, A.A., Ismail, R.A., and Mohsin, M.H., 2020, Antibacterial and cytotoxic activities of cerium oxide nanoparticles prepared by laser ablation in liquid, *Environ. Sci. Pollut. Res.*, 27 (24), 30479–30489.

[42] Wan Isahak, W.N.R., Che Ramli, Z.A., Ismail, M.W., Ismail, K., Yusop, R.M., Mohamed Hisham, M.W., and Yarmo, M.A., 2013, Adsorption-desorption of CO_2 on different types of copper oxides surfaces: Physical and chemical attractions studies, *J. CO_2 Util.*, 2, 8–15.

[43] Zgurskaya, H.I., Löpez, C.A., and Gnanakaran, S., 2015, Permeability barrier of gram-negative cell envelopes and approaches to bypass it, *ACS Infect. Dis.*, 1 (11), 512–522.

[44] Alenazy, R., 2022, Drug efflux pump inhibitors: A promising approach to counter multidrug resistance in gram-negative pathogens by targeting AcrB Protein from AcrAB-TolC multidrug efflux pump from *Escherichia coli*, *Biology*, 11 (9), 1328.

[45] Ma, X., Zhou, S., Xu, X., and Du, Q., 2022, Copper-containing nanoparticles: Mechanism of antimicrobial effect and application in dentistry-a narrative review, *Front. Surg.*, 9, 905892.

[46] Akpasi, S.O., and Isa, Y.M., 2022, Effect of operating variables on CO_2 adsorption capacity of activated carbon, kaolinite, and activated carbon–kaolinite composite adsorbent, *Water-Energy Nexus*, 5, 21–28.

[47] Zheng, X., Hu, L., Zhu, J., He, J., and Liu, X., 2022, Effect of the dispersion behavior of cerium oxygen species on CO_2 adsorption performance, *J. Environ. Chem. Eng.*, 10 (1), 106986.

[48] Yoshikawa, K., Kaneeda, M., and Nakamura, H., 2017, Development of novel CeO_2-based CO_2 adsorbent and analysis on its CO_2 adsorption and desorption mechanism, *Energy Procedia*, 114, 2481–2487.

[49] Shinde, S.K., Dubal, D.P., Ghodake, G.S., Gomez-Romero, P., Kim, S., and Fulari, V.J., 2015, Influence of Mn incorporation on the supercapacitive properties of hybrid CuO/$Cu(OH)_2$ electrodes, *RSC Adv.*, 5 (39), 30478–30484.